Eur. Phys. J. Appl. Phys. **93**, 10504 (2021)

https://doi.org/10.1051/epjap/2020200243

THE EUROPEAN PHYSICAL JOURNAL APPLIED PHYSICS

Regular Article

# The laser lightning rod project★

Thomas Produit[1], Pierre Walch[2], Clemens Herkommer[3,4], Amirhossein Mostajabi[5], Michel Moret[1], Ugo Andral[1], Antonio Sunjerga[5], Mohammad Azadifar[9], Yves-Bernard André[2], Benoît Mahieu[2], Walter Haas[6], Bruno Esmiller[7], Gilles Fournier[7], Peter Krötz[3], Thomas Metzger[3], Knut Michel[3], André Mysyrowicz[2,8], Marcos Rubinstein[9], Farhad Rachidi[5], Jérôme Kasparian[1,10], Jean-Pierre Wolf[1], and Aurélien Houard[2*]

[1] Groupe de Physique Appliquée, Université de Genève, Ch. de Pinchat 22, 1211 Geneva 4, Switzerland
[2] LOA, ENSTA Paris, CNRS, École Polytechnique, Institut Polytechnique de Paris, 828 Bd des Maréchaux, 91762 Palaiseau, France
[3] TRUMPF Scientific Lasers GmbH + Co. KG, Feringastr. 10a, 85774 Unterföhring, Germany
[4] Department of Physics, Technische Universität München, James-Franck-Str. 1, 85748 Garching, Germany
[5] EMC Laboratory, Electrical Engineering Institute, Swiss Federal Institute of Technology, 1015 Lausanne, Switzerland
[6] Swisscom Broadcast AG, Ostermundigenstrasse 99, 3050 Bern, Switzerland
[7] ArianeGroup, France
[8] André Mysyrowicz Consultants, 6 Rue Gabriel, 78000 Versailles, France
[9] Institute for Information and Communication Technologies, University of Applied Sciences and Arts Western Switzerland, 1401 Yverdon-les-Bains, Switzerland
[10] Institute for Environmental Sciences, Université de Genève, Bd Carl Vogt 66, 1211 Geneva 4, Switzerland

Received: 22 July 2020 / Received in final form: 21 October 2020 / Accepted: 23 October 2020

**Abstract.** Lightning is highly destructive due to its high power density and unpredictable character. Directing lightning away would allow to protect sensitive sites from its direct and indirect impacts (electromagnetic perturbations). Up to now, lasers have been unable to guide lightning efficiently since they were not offering simultaneously terawatt peak powers and kHz repetition rates. In the framework of the Laser Lightning Rod project, we develop a laser system for lightning control, with J-range pulses of 1 ps duration at 1 kHz. The project aims at investigating its propagation in the multiple filamentation regime and its ability to control high-voltage discharges. In particular, a field campaign at the Säntis mountain will assess the laser ability to trigger upward lightning.

## 1 Introduction

Lightning fascinates due to its destructive power, which also makes it a major natural risk. It is estimated that casualties varying from 6000 to 24 000 people per year are related to lightning strikes worldwide [1]. Lightning also causes power outages, forest fires and damages to electronic systems and infrastructure, with associated costs of billions of Euros each year [2,3]. In spite of considerable progress, lightning protection still relies on the nearly 300-years-old concept of the lightning rod, as invented by Benjamin Franklin [4]. However, many situations such as mass gatherings or temporary storage of dangerous materials require to temporarily deploy lightning protection at locations that do not need and/or cannot afford a permanent lightning rod. Furthermore, the operation of rocket launchpads and airport runways and taxiways is not compatible with the permanent presence of the tall towers required to protect large volumes and/or wide areas with a classical lightning rod. A protection system that could be briefly removed on-demand, e.g., switched off at each airplane landing, would have much less impact on the airport operations. Furthermore, lightning rods only protect against direct effects of lightning. By attracting lightning strikes to conduct their transient current to the ground, they may even increase the incidence and severity of indirect effects, namely electromagnetic perturbation and over-voltage on electric or electronic devices and appliances. Preventing such indirect effects would require either to prevent the occurrence of lightning strikes or to attract them away from the facility to be protected.

Depending on the effective height of a strike object (which depends on its physical size and on the topography of the terrain on which it is erected), it can be struck essentially by downward lightning, by upward lightning or by a comparable fraction of each [5]. Many of the damages to wind turbines, communication towers and tall buildings can be attributed to upward lightning. Upward lightning strikes are also known to exhibit characteristics similar to those of lightning triggered by aircraft and rockets [6].

Small rockets trailing a grounded conducting wire have been used to trigger lightning for research purposes since

★Supplementary material is available in electronic form at https://www.epjap.org/10.1051/epjap/2020200243

* e-mail: aurelien.houard@ensta-paristech.fr

the 1960s [7,8]. The success of this approach strongly depends on the location and the stage of the thunderstorm as well as the electric field close to the ground at the time of the triggering attempt. Launchpads are generally fixed and typically limited to $5-10$ rockets, although mobile launchpads have also been used. Furthermore, the rockets fall back to the ground regardless of the success of the triggering attempt. Finally, while the wire melts away during successful attempts, a few hundred meters of conductive wire fall to the ground with the rocket in the case of unsuccessful launches, implying risks for personnel and equipment on the ground.

A continuously operating technique to trigger lightning would therefore be highly desirable. Lasers were identified very early as candidates for this purpose. The first tests performed in the 1970s using "long" laser pulses of several nanoseconds or more demonstrated the guiding of megavolts discharges with lengths of up to 2 m [9,10]. An attempt to trigger and guide natural lightning was made by Uchida et al. in 1999 using a combination of three lasers with a kJ-level energy to form a 2 m long plasma spark at the tip of an experimental tower [11]. The researchers reported two successful events, but this low number of events did not lead to conclusive proof of the effectiveness of the lightning triggering technique. This approach was progressively abandoned because of the discontinuous profile of the plasma generated with such "long" IR or mid-IR pulses through avalanche ionization and the huge laser energy required to extend the laser-generated plasma column beyond a few meters.

In contrast, sub-100 fs laser pulses are short enough to prevent electron avalanche. The generated plasma remains therefore transparent to the laser pulse. As a consequence, ionizing self-guided filaments can exceed 100 m in length. Filamentation is a self-guided, non-linear propagation mode that relies on the dynamic balance between the optical Kerr effect that tends to focus the laser beam and self-defocusing, mainly due to the plasma generated when the pulse intensity becomes sufficiently high [12–16]. It results in the long range propagation of a pulse with multi-GW peak intensity. A plasma track and a low air density channel are left in the wake of the pulse. These ionized light filaments can be generated at a distance of several kilometers [17], and can cover a length of more than a hundred meters [18] by an adequate choice of the laser parameters. They can be directed to any position in the atmosphere by sweeping the beam using a steering mirror. In the 2000s, several groups demonstrated their capability to trigger high-voltage discharges over several meters with laser pulses of only 100 mJ [19–21]. By electrically connecting two electrodes that were several meters apart, the laser filaments reduce the breakdown voltage by 30% [21], triggering the discharge in conditions that would not have allowed them to without the laser. These triggered discharges are guided along the laser filaments rather than following the erratic path typical of a classical electric discharge. Furthermore, filaments are able to divert a discharge from its preferential path [22].

Based on these successful results on a laboratory scale, a mobile, femtosecond-terawatt laser, "Teramobile", was developed [23,24]. In a field campaign at the Langmuir Laboratory of the New Mexico Tech on the South Baldy Peak, micro-discharges synchronized with the laser pulses were detected, showing that laser filaments initiated corona discharges in thunderclouds [25]. However, the short lifetime of plasma filaments (typically a few ns) prevented the initiation of upward leaders similar to the mechanism of rocket triggering. Increasing the plasma lifetime by heating the filament plasma with an additional, high-energy nanosecond laser was proposed by several groups [19,26–29]. However, this requires an additional laser of high energy, typically in the joule range. Coupling such a beam into the filament proved to be unpractical over distances exceeding a few meters.

On the other hand, filamentation initiates a low-density (air-depleted) channel [30–33]. For a low-repetition rate multi-TW laser, the air density is initially reduced by a factor of 5 over a typical length of a few meters. The density depletion still amounts to typically 10% of the ambient pressure after 1 ms. These straight, low-density channels favor the triggering and guiding of electric discharges in the atmosphere at a 60% reduced voltage [22,34]. At repetition rates in the kHz range, the depletion of the air density due to filamentation is amplified by a cumulative effect [32]. As a result, increasing the repetition rate of 100 mJ, 1030 nm laser pulses from 10 Hz to 1 kHz reduces the laser-induced breakdown voltage by a factor of 3 [35]. Therefore, a terawatt laser at a kilohertz repetition rate would allow the formation of a permanent low-density channel likely capable of guiding discharges over long distances.

Based on these results, we decided to investigate the impact of laser filamentation at a kHz repetition rate on lightning strikes, in real scale. More specifically, within the Laser Lightning Rod (LLR) project [36] we focus on developing a kHz-terawatt laser system and assessing its ability to stimulate upward lightning flashes from the grounded, 123 m tall telecom tower at Säntis, Switzerland, in order to initiate and guide the lightning strikes.

## 2 High peak- and average-power laser source

Research on laser filamentation for atmospheric applications has long been based on Ti:Sa lasers due to the high peak power of their pulses with a duration on the order of tens of femtoseconds [15,16,24]. These femtosecond lasers are well suited to study the formation and the dynamics of laser filaments, because the 3 GW critical power for self-focusing in air [37] is already reached at energies of a few mJ, limiting the cost, effort, and complexity of the experiment [16].

However, the average power typically provided by commercial Ti:Sa systems is limited to a few watts. The 30% quantum defect of Ti:Sa induces a substantial heat load, the dissipation of which is limited by the finite thermal conductivity of sapphire. Furthermore, the radiative lifetime of the $Ti^{3+}$ ions is as short as 3 µs to 4 µs [38], requiring complex and expensive pumping schemes around 500 nm.

Yb-doped laser crystals have emerged as the material of choice for high-average-power applications since the

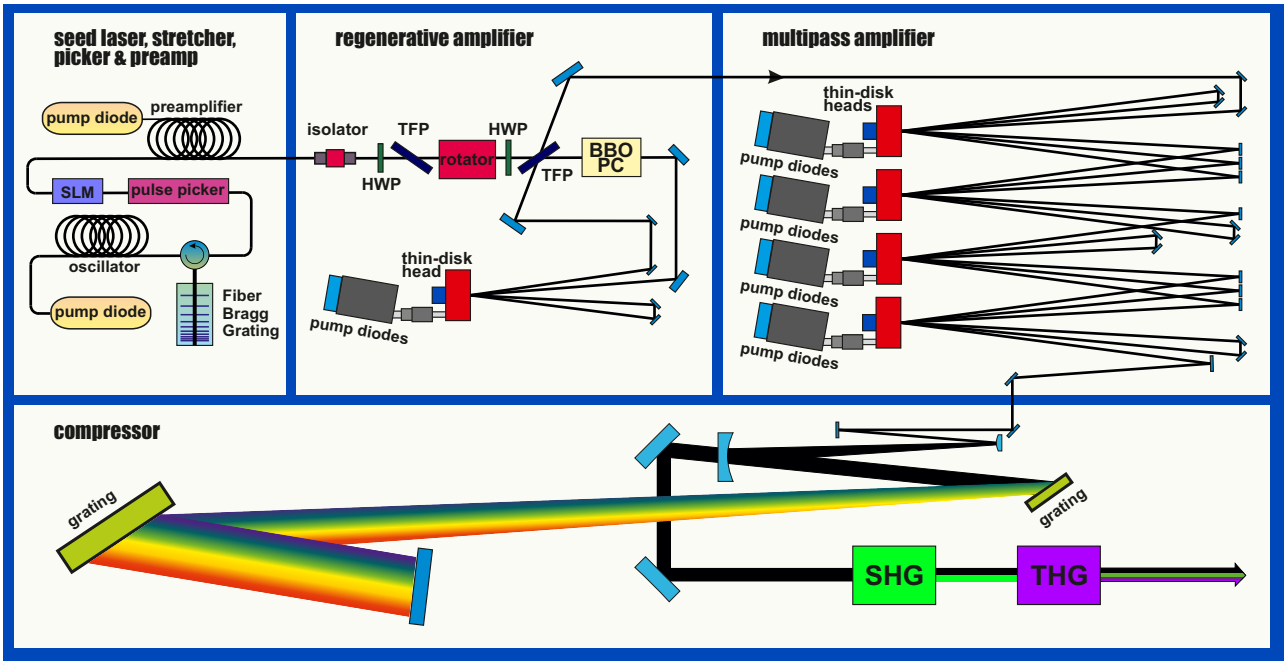


**Fig. 1.** Scheme of the LLR thin-disk based CPA laser system. The main laser components are based on the industrial solutions from TRUMPF Laser GmbH. The seed pulses are stretched in a chirped fiber Bragg grating (CFBG) and pre-amplified in an active fiber. The energy of the chirped pulses is increased in the subsequent regenerative amplifier delivering >200 mJ of pulse energy. The multipass amplifier consists of four thin-disk laser heads and it is capable of boosting the pulse energy to the Joule level. Pulse recompression down to $\leq 1$ ps pulse duration is performed in a Treacy-type grating-based compressor. SLM: Spatial Light Modulator; BBO-PC: Beta Barium Borate based Pocket Cells; HWP: Half-Wave Plate; TFP: Thin Film Polarizer; SHG: Second Harmonic Generation; THG: Third Harmonic Generation.

advent of very powerful and brilliant InGaAs pump laser diodes [39], providing kilowatts of optical power around the main absorption band of Yb-doped crystals at 940 nm. Exceptionally low heat is generated owing to the small quantum defect ($\sim$9%), while their long fluorescence lifetime ($\sim$0.9 ms) and excellent thermal conductivity allow for cw pumping and operation at very high average power levels [40].

The thin-disk geometry has been established as one of the most successful candidates for high-power scaling, providing multikilowatt laser output power [39]. Invented in 1993 by Adolf Giesen [41], the technology has been matured and industrialized by TRUMPF Laser GmbH over more than two decades, focusing on industrial applications. The main advantage of the thin-disk is in the very efficient cooling capacity, enabled by thermally contacting the large disk surface by means of diamond or copper heat sinks, which results in a one-dimensional heat flow, co-directional with the laser-optical axis, thereby greatly minimizing thermal lensing and thermally-induced wavefront aberrations. From a single disk, up to 4 kW in the fundamental mode [42] and up to 12 kW in multimode operation can be achieved, with an optical efficiency as high as 70% [43].

Recently, the thin-disk technology was also implemented in the field of ultrafast lasers. In particular, large mode areas allow for high pulse energies at reasonable fluences while the short propagation distance through the gain medium keeps the nonlinearities low. With the advent of "cold" material processing and micromachining, the demand for powerful and highly energetic ultrashort pulsed lasers has pushed their development in the industrial domain, leading to commercial micromachining lasers with pulse energies up to several millijoules at repetition rates of hundreds of kHz, with pulse durations well below 1 ps [44,45]. Driven by the need for powerful pump lasers for optical parametric chirped pulse amplifiers (OPCPA), scientists applied the industrial thin-disk laser components to build ultrafast lasers aiming at tens of millijoules of pulse energy at repetition rates between 5–10 kHz [46]. Recently, pulse energies above 200 mJ at multikilowatt average powers have been demonstrated from advanced thin-disk based regenerative amplifiers [47].

The layout of the LLR laser system is shown in Figure 1. The seed pulses are produced by an industrial fiber-based ultrafast laser, typically used for micromachining (TruMicro 2000). The ultrashort pulses are stretched by a chirped fiber Bragg grating and pre-amplified in an active fiber. A Dira 200-1 regenerative amplifier [48] serves as the first high-power amplification stage, featuring a thin-disk laser head, a BBO-based Pockels cell, and a cavity supporting only the fundamental mode in a ring-type configuration. The output pulse energy of 200 mJ is further amplified in a specifically-developed amplifier implementing another four thin-disk laser heads in a multipass configuration. Each thin-disk laser head of the multipass amplifier can be pumped with more than 10 kW of optical power. Here, multiple thin-disk passes are achieved

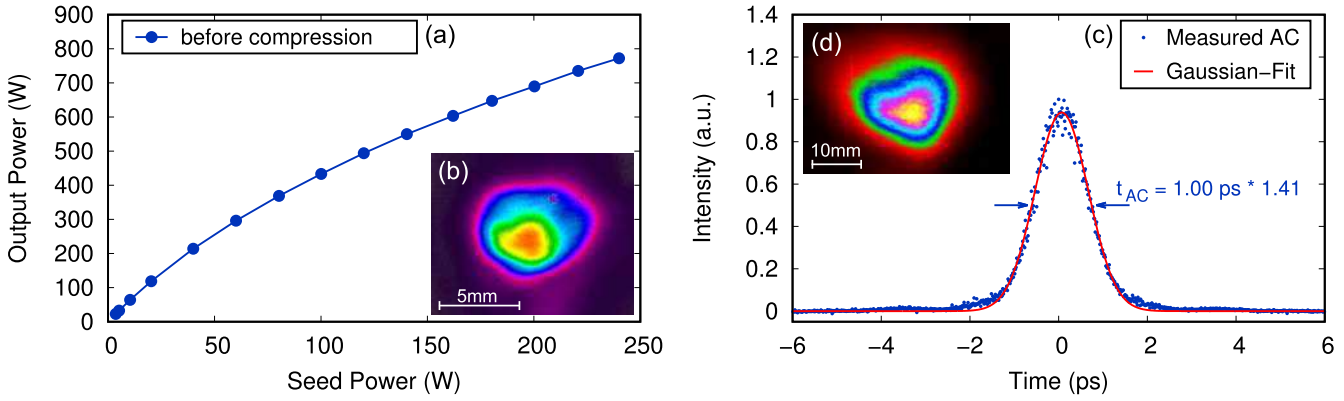


**Fig. 2.** Characterization measurements of the laser system. (a) Amplification slope of the multipass amplifier. The measured output power is plotted as a function of the seed power. (b) Near-field beam profile of the uncompressed output of the multipass amplifier. (c) Measured autocorrelation trace of the compressed output pulses at 720 mJ pulse energy. Assuming a Gaussian temporal pulse shape, the pulse duration is 1 ps. (d) Near-field beam profile of the compressed output.

by spatially displacing the signal beam rather than using a closed optical resonator with an electro-optical switch. In this way, an arbitrary signal can be amplified to pulse energies up to the Joule level, while the beam diameter can be scaled with the pulse energy, only limited by the aperture of the optics and the thin-disk. Carefully designed refractive optics are implemented in order to ensure a collimated and sufficiently large signal beam during its propagation through the multipass amplifier, thereby operating below the laser-induced damage threshold of optical components. Finally, pulse recompression is achieved by double-passing a grating compressor in Treacy-type near-Littrow configuration, supporting a spectral bandwidth sufficient to reach a Fourier-limited pulse duration well below 1 ps [49]. Additionally, a spatial light modulator (SLM) can tune the residual dispersion of the output pulses and adjust the pulse duration by applying temporal chirp.

High-energy amplification was first demonstrated with two laser heads in the main multipass amplifier [50]. The pulse energy was boosted from 230 mJ to 600 mJ before pulse compression, i.e., an amplification factor of 2.6. By making use of all four laser heads, the pulse energy has been increased further towards the 1-Joule level (Fig. 2a). At 1 kHz repetition rate, the average output power before compression reaches around 800 W, translating to 800 mJ of pulse energy before compression. After recompression, the pulse energy remains at 720 mJ, limited by the diffraction efficiency of the compressor gratings [51]. The pulse duration of 1 ps (Fig. 2c) is mainly limited by the available spectral bandwidth of the high-energy output pulses due to gain narrowing [52]. Spectral filtering inside the regenerative amplifier cavity [53] or spectral shaping of the seed pulses [54] could in the future allow shorter pulse durations. Typical spatial near-field beam profiles of the compressed and the uncompressed output laser beam are shown in Figures 2b and 2d. Note that a magnification factor of 4 is to be considered for the mode size of the compressed beam ($D \approx 28.8$ mm) with respect to the uncompressed beam ($D \approx 7.2$ mm).

Besides the fundamental wavelength of 1030 nm, the second and third harmonics at 515 nm and 343 nm, respectively, are also provided via SHG and THG conversion stages after the compressor. Conversion efficiencies of up to 45% for SHG and 27% for THG have been achieved by using 50 mm diameter LBO crystals (Crystal Laser SA, France) with this laser system [55]. Furthermore, the use of UV could drastically reduce inverse Bremsstrahlung, that is proportional to the wavelength squared [56], maximizing the ability of the ps-range pulses generated by the laser to produce avalanche-free filaments [57].

## 3 HV discharges triggered by dual- and triple-frequency laser filaments at high repetition rate

We compared the effect on high-voltage discharges of the low-density channel created by a laser pulse at the 1030 nm fundamental wavelength, to the one created by a dual-laser pulse combining the fundamental and the SHG by using an interferometer arrangement [58]. The phase shift induced by the low-density channel on a transverse probe laser is characterized using a wavefront sensor. The partial conversion of the pulse into the SHG increases this phase shift $\phi$, indicating that the air density is more depleted. Furthermore, the depleted channel is longer (Figs. 3a and 3b). One can therefore expect that frequency-doubling the laser enhances the ability of filaments to trigger high-voltage discharges [34].

Indeed, the maximum breakdown length between two spherical electrodes under 26 kV voltage (see Fig. 3c), increases when the laser is frequency-converted to the second and third harmonics. It is limited to 18 mm for 120 mJ pulses at 1030 nm, but reaches 21 mm when combining 66 mJ at 1030 nm and 54 mJ at 515 nm. It even increases to 25 mm for 25 mJ pulses at 343 nm [55]. These preliminary results seem to indicate that, given a fixed amount of laser energy, upconverting the laser light to create dual- or triple-frequency filaments is beneficial to increase the breakdown distance, hence to increase the efficiency of electric discharge triggering. In other words, the increased triggering efficiency does more than compensating the

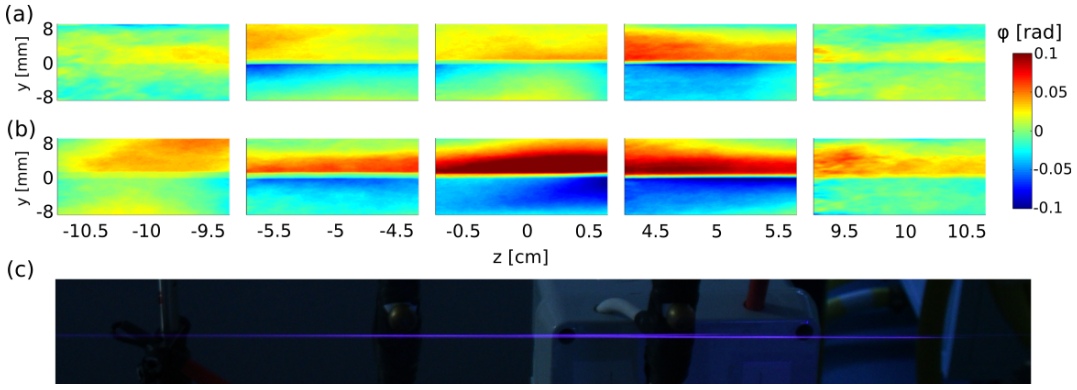


**Fig. 3.** Phase shift map around the laser filaments, measured at different propagation distances $z$, 10 µs after the laser pulses, for (a) a laser pulse at 1030 nm with an energy of 120 mJ ; (b) a dual-color laser pulse of 66 mJ at 1030 nm and 54 mJ at 515 nm. (c) Still image of the filament between the two electrodes of the HV generator without applied voltage on the electrodes. Position z = 0 corresponds to the center of the image. The laser comes from the left.

laser energy losses of the frequency-conversion process. However, effects occurring due to propagation of the laser beam through hundreds of meters of atmosphere may reverse these conclusions. Experiments are in progress to determine the optimum mode of operation for the long-distance generation of laser filaments.

## 4 Lightning research at the Säntis observatory (Switzerland)

Switzerland has a long tradition of lightning studies. Starting in the 1950s, extensive experimental data on lightning were recorded for nearly 3 decades by Berger and his team [59] on two instrumented towers on the Mount San Salvatore, Southern Switzerland. The obtained results suffered, however, from the technological limitations of the instruments limited by the frequency bandwidth of a few hundred KHz at the time.

The field experiments of the LLR project will be performed at the top of the Säntis Mountain (Switzerland), located at 47.249 44 °N, 9.343 69 °E, and 2481 m altitude (Fig. 4a). This site has a weather station active since 1882. The summit is accessible by a cable car since 1935, and hosts since 1955 a radio/TV transmitting station. In 1998, the station was upgraded and the current 123 m tall tower was built. It has been used for lightning research purposes since 2010. Indeed, the Säntis is one of the lightning hotspots in Europe, with around 100 events/year [60], mostly concentrated between May and August. Typically the only snow free months are August and September. Typical Summer temperatures (0 °C to 10 °C), diurnal amplitudes (∼6 °C), relative humidity (RH, 80% – 90%) and wind gusts up to almost 180 km /h impose severe constraints on experiments. This is especially the case for a sensitive instrument like a high-power ultrashort laser.

Since 2010, two sets of instruments measure both, currents and current derivatives at 24 m and 82 m above ground level (Fig. 4b), under remote control and monitoring. Rogowski coils measure the low-frequency current from 10 mHz up to 3 MHz, while multigap B-dot sensors provide current-derivative waveforms with a 20 MHz bandwidth. Their design is based on that proposed by Baum, Breen, Giles, O'Neil, and Sower [62,63]. The measured signals are transmitted over optical fibers to a National Instruments PXI-5122 high-speed digitizer that records each lightning flash over a measurement time window of 2.4 s at a sampling rate of 50 MS/s [60,64]. The electromagnetic fields are measured by wideband electric and magnetic field sensors as well as a field mill installed inside a dome next to the tower. Wideband field sensors are also installed at a 14.7 km distance, on the roof of a 20 m tall building. The wideband vertical electric field is also measured at a distance of 380 km, in Northwestern Austria, by a flat-plate antenna belonging to the Austrian Lightning Detection and Information System (ALDIS).

Besides the electromagnetic field measurement sensors, a Phantom high-speed video camera was installed in 2018 on the Kronberg mountain, some 4 km North of the Säntis tower (see Fig. 4a). The camera overlooks the tower from a storage room at the Kronberg Luftseilbahn. Figure 5 and Supplementary Material respectively display a sample frame and a movie of an upward positive flash recorded on July $2^{nd}$, 2019.

Several other sensors have been temporarily installed near the Säntis. These include a lightning mapping array (LMA) that locates in 3D VHF sources along the lightning channel, inside as well as outside the clouds. An interferometer, manufactured by New Mexico Tech [65], was installed in Summer 2019. It will be used again to evaluate the impact of the laser on the lightning activity, by mapping VHF sources in the two angular spherical coordinates. Other recently installed sensors include scintillation detectors to measure high energetic X-ray and Gamma-ray radiation.

Since the start of the operation of the modern lightning measurement system at the Säntis Tower in 2010, almost 1000 flashes have been recorded and analyzed [60]. They consist of 85% negative, 12% positive and 3% bipolar flashes. Almost all flashes (about 97% ) are of the upward type. Most results obtained at the Säntis are related to

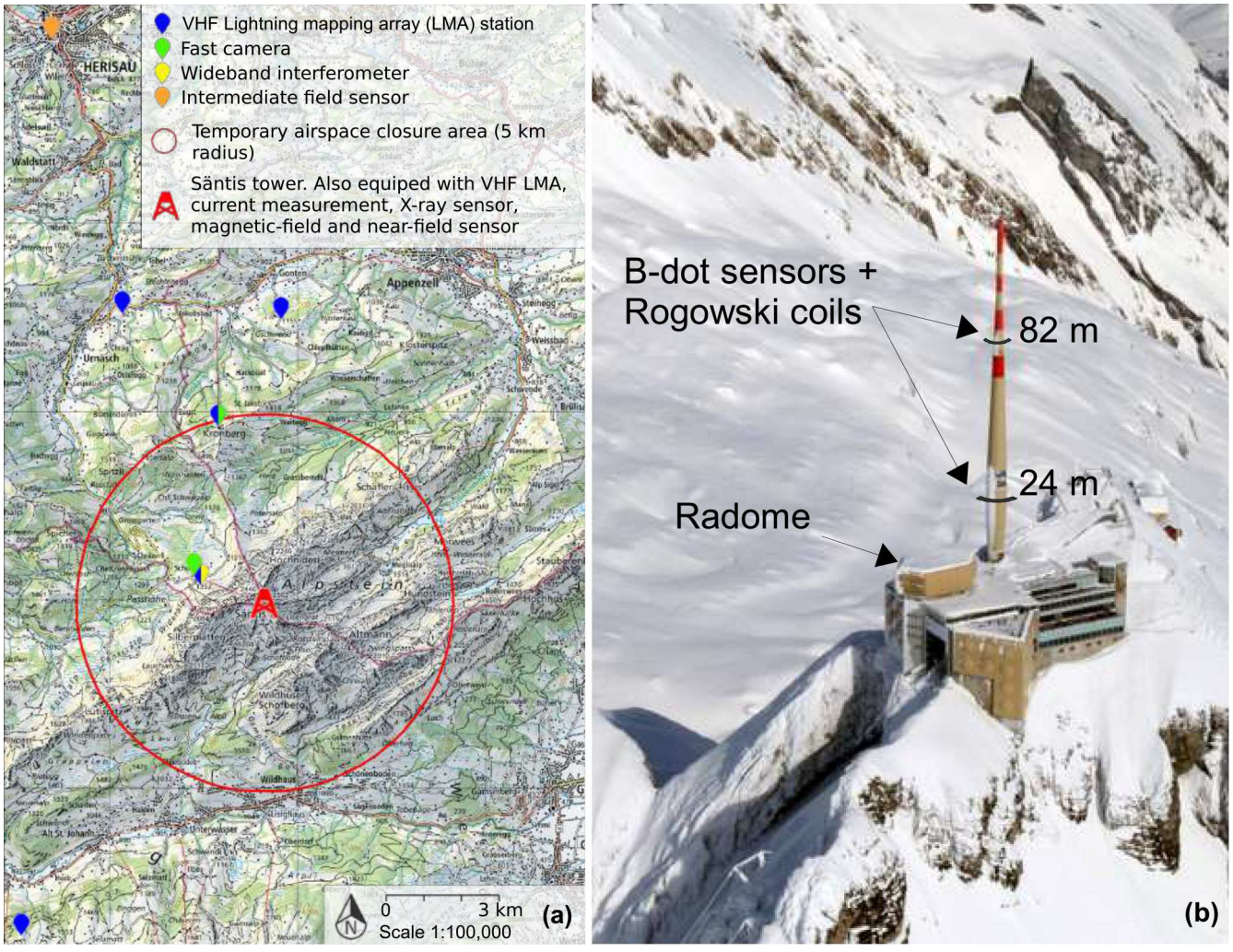


**Fig. 4.** Experimental site: Säntis station. (a) Situation map, including auxiliary instruments and no-fly zone – background map Swisstopo. (b) General view of the station and location of the Rogowski coils and B-dot sensors measuring lightning currents – background image from [61].

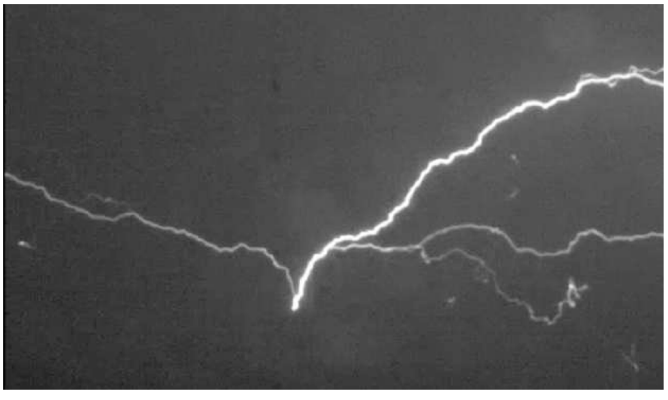

**Fig. 5.** 100 µs resolution image of an upward lightning strike on the Säntis tower on July 2*nd*, 2019, observed from the Kronberg mountain. See Supplementary Material for the full sequence.

the physics of lightning, among which the study of processes in upward negative cloud-to-ground flashes [66,67], the characterization of upward positive cloud-to-ground flashes [68], propagation of lightning electromagnetic fields over irregular terrain [69], and lightning-ionosphere interactions [70]. In addition, a significant fraction of the activity regards the evaluation and development of lightning detection and forecasting, in particular the performance analysis of the European Lightning Detection Network for Upward Flashes [14,71] and the forecasting of lightning occurrence using machine learning (ML) [72].

The latter work aims at deciding the most favorable laser activation times as well as a posteriori assessing the laser effect on the lightning initiation. Using a ML approach, excellent predictors for the occurrence of lightning during three subsequent 10-min intervals and within a radius of 30 km were produced from four local atmospheric measurements: the surface air pressure at station level (QFE), the air temperature 2 m above the ground, the relative air humidity, and the wind speed [72]. These parameters, together with the lightning activity data from MeteoSwiss, were considered for years 2006–2017 with

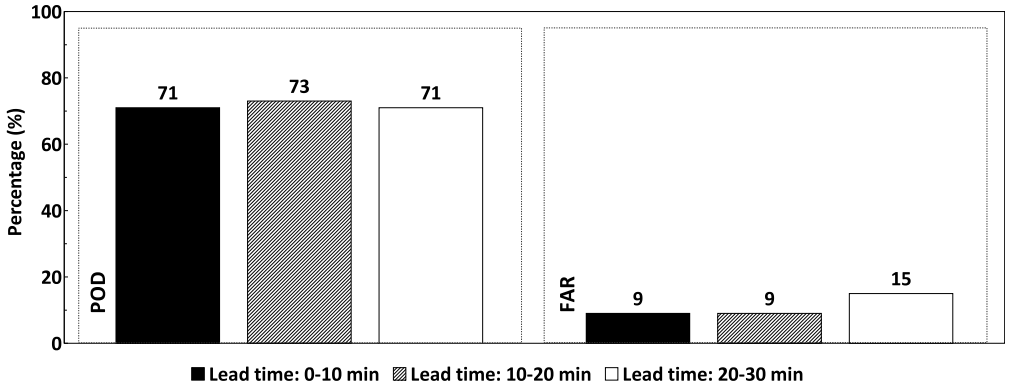


**Fig. 6.** Evaluation of the skill of warnings generated by the machine learning model for long-range lightning activity and for three ranges of lead times at the Säntis station (POD: Probability of Detection and FAR: False Alarm Ratio).

10 min granularity. Each 10-min interval was labeled as a lightning-active sample if at least one flash was recorded in that interval within 30 km distance from the tower [72]. Then, the machine was trained with some portion of the data (training set) to predict the lightning activity given the meteorological observations. Once trained, it used the remaining part of the data (testing set) to test the accuracy of the warnings. The proposed ML model reaches a Probability of Detection (POD) exceeding 70% and a False Alarm ratio (FAR) below 10% (Fig. 6) [72]. POD is defined as the ratio of the events correctly hit by the model to the total number of observed events (lightning-active samples). These results confirm that the model has statistically-considerable predictive skill for lead times up to 30 min.

## 5 The Laser Lightning Rod experiment implementation at Säntis

For the laser to initiate upward lightning from the tip of the Säntis tower, the filamentation onset should be close to the tower top. To protect the laser against an adverse environment, ensure laser safety of the public in the station, and comply with environmental constraints, the experiment needs to fit in the existing buildings. Therefore, the laser will be located in the radome $\sim$20 m away from the tower (Fig. 7a). More specifically, the laser system, with a footprint of 3 m $\times$ 8 m, will be installed on the $8th$ floor of the radome building hosting telecom antennas as well as the electric distribution of the station, including additional emergency power generators. However, this area does not offer the clean conditions of a laser laboratory. Furthermore, its temperature typically varies between 5 and 24°C over the day during the summer. Therefore, the laser will be further sheltered in a dedicated air-tight polyester tent equipped with an air conditioning system stabilizing the temperature at $20 \pm 2$°C and 50% relative humidity.

The laser output beam will be directed downwards to the terrace through the radome skin in a 20 cm diameter metal tube, leading the beam into an isolated aluminium housing where a 4" folding mirror directs the beam into a beam-expanding sending telescope featuring a 7.14 magnification ratio. It consists of an additional folding mirror, a secondary 85 mm spherical mirror and a 430 mm diameter off-axis parabolic primary mirror (Fig. 7b). The final beam diameter is 250 mm at $1/e^2$. Motorized linear stages on the secondary mirror allow to slightly focus the beam ($100\,\text{m} < f < \infty$) close to or beyond the tower tip. The sending telescope has also been designed such that the beam exit matches the 7° angle with respect to nadir, as required to reach close to the tower tip. All optical components are tri-band coated (1030 nm, 515 nm and 343 nm) in order to allow experiments with filaments at the fundamental wavelength as well as with the second and third harmonics. The filament onset distance is tuned by controlling the spatial and temporal focusings. The former is obtained by adjusting the telescope focus. The latter is achieved by detuning the SLM so as to pre-chirp the pulse, and adjust the initial pulse duration.

The optical quality of the telescope has been characterized at $\lambda = 632.8$ nm by measuring the wavefront distortions after the propagation through the entire telescope (2 mirrors), with the use of a large calibrated plane mirror that allowed a double-pass in the telescope. The wavefront distorsion mostly corresponds to higher-order Zernike terms, and it stays below $\lambda/2$ peak to valley (PtV) for $f = \infty$. Simulations using Code V predict that the additional wavefront distorsion brought by shifting the secondary mirror to focus the beam is negligible down to $f = 200$ m and limited to $\lambda$ at $f = 100$ m. The wavefront quality at the focus will therefore not be limited by the optical setup, especially considering that the planned experiments in thunderstorms imply the propagation of the beam over more than 100 m of highly turbulent air, with associated wavefront distorsions of at least $3\lambda$.

The experiment implementation imposes 13 m propagation from the laser output to the expanding telescope. A critical issue is therefore the potential self-focusing and filamentation ahead of the latter, resulting in damage on the mirrors. This self-focusing, that critically depends on the pulse peak intensity [73,74] will be controlled with an adequate pre-chirping of the pulse, as initially proposed by the Teramobile group [23]. Indeed, preliminary tests show that chirping a 650 mJ, 1 ps pulse to 4 ps is sufficient to shift the filamentation onset distance from 8 m to

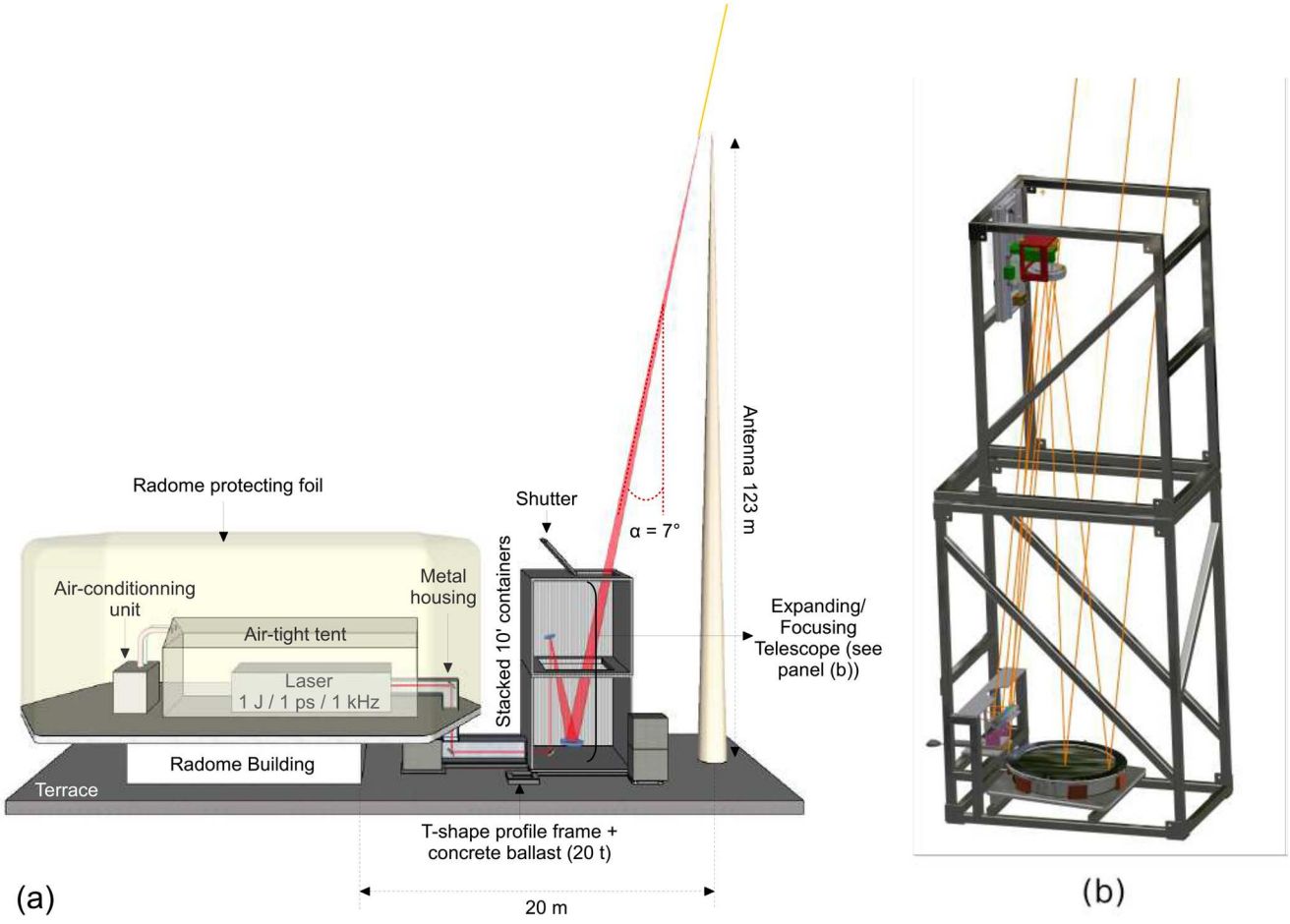


**Fig. 7.** (a) Principle of the general layout of the laser experiment implementation at Säntis (not to scale). (b) Schematic drawing of the sending telescope.

15 m, beyond the sending telescope. One should note that group velocity dispersion and temporal lensing effect will be negligible for a kilometer range propagation of a 1 ps pulse, similarly to the experiment in reference [18].

To preserve the beam quality by ensuring thermal stability, as well as to protect optics from precipitation and ensure laser safety, the beam will be sheltered in a thermally isolated aluminium construction (Fig. 7b). A first section will lie horizontally from the radome building to the telescope housing system. The latter will be made of two stacked customized 10' containers. The whole construction will be anchored on a T-profile frame and stabilized against tilting and sliding by 20 concrete blocks of 930 kg each, a setup dimensioned to withstand winds up to 200 km/h.

Finally, open-air laser experiments require addressing laser safety, both for air traffic and for the public at and around the Säntis station. A no-fly zone (see Fig. 4a) has been defined in coordination with the Federal Office of Civil Aviation and the Swiss air navigation service provider (Skyguide) and will be activated before each experiment. Furthermore, the laser will be installed in a private zone of the Säntis station, keeping the public beyond the minimal horizontal distance of 3 m required by Swiss regulations [75]. Finally, the laser beam will be sheltered all over its way to the end of the sending telescope, ensuring that any reflection or scattering can hit neither operators nor the public.

## 6 Measurement strategy

Lightning is highly stochastic. The atmospheric conditions are rapidly changing during thunderstorms and cannot be fully characterized. The assessment of a laser effect on lightning therefore requires a careful statistical analysis, the significance of which is critically impacted by the laser firing sequence. This sequence should provide laser-free reference periods of sufficient duration, with similar atmospheric conditions and natural probability of lightning strikes. Furthermore, the firing sequence should limit biases related to the evolution of the weather conditions during the experiment, and allow to compare various laser conditions, including the use of harmonics, the duration of laser pulse bursts, focusing, or pulse duration (via the initial chirp). Furthermore, in the absence of a 100% reliable forecast of the atmospheric state during the thunderstorm, the firing sequence has to adapt in real time to the actual evolution of the situation.

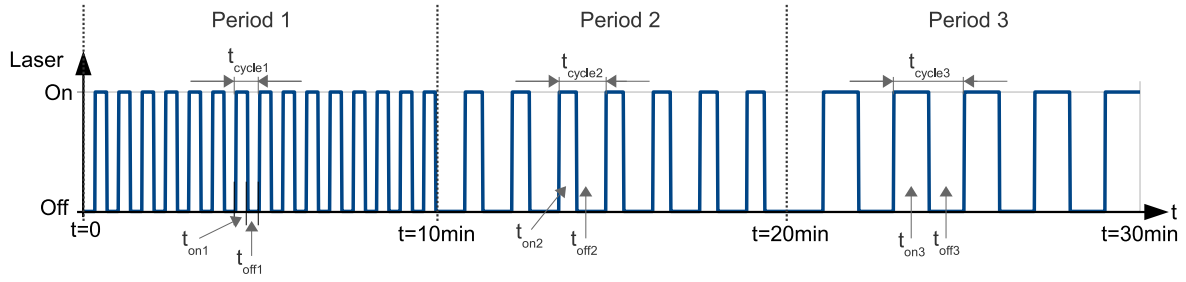


**Fig. 8.** Principle of the laser firing sequencing.

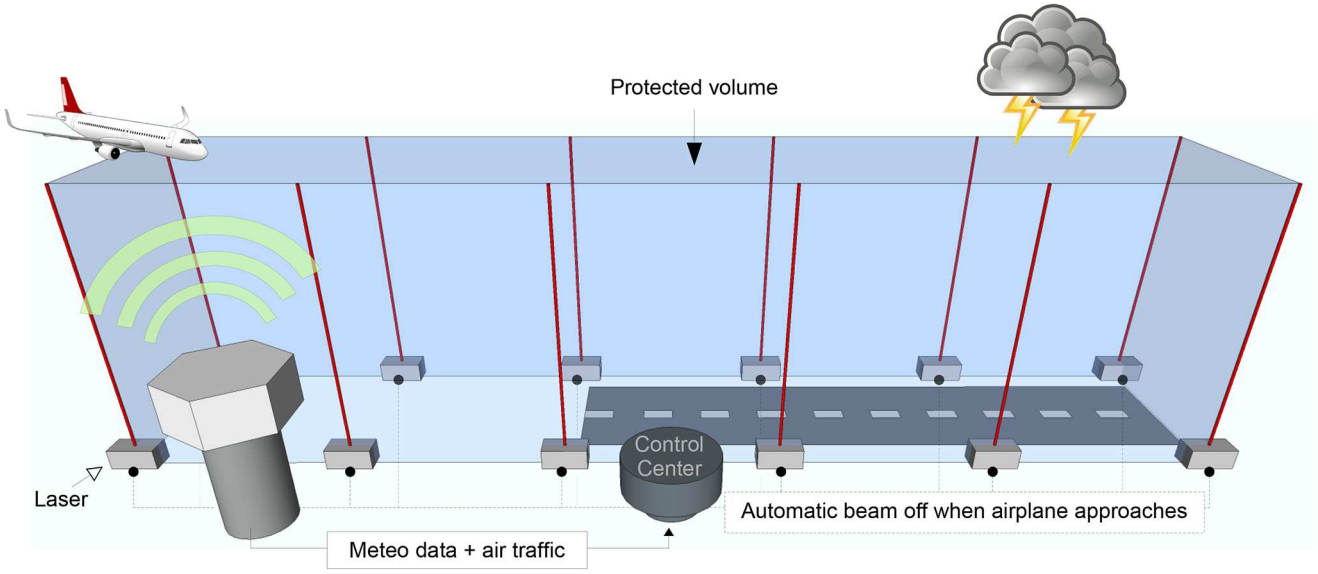


**Fig. 9.** Potential laser network geometry for aircraft protection during landing and take-off.

Measurements will be initiated as soon as MeteoSwiss forecasts a risk of thunderstorms. The experimental sequence will be decomposed into periods of 10 min corresponding to the granularity of MeteoSwiss data. During each period, cycles of constant duration $T_{\text{cycle}} = T_{\text{on}} + T_{\text{off}}$ will be repeated (Fig. 8), alternating laser ON and OFF times. In each cycle, the laser active time ($T_{\text{on}}$) will last at least several seconds to tens of seconds to allow cumulative effects to develop. The reference time will then be adjusted to $T_{\text{off}} = T_{\text{cycle}} - T_{\text{on}}$. It should last at least a few seconds to allow the wind to renew the air parcel swept by the laser beam, so that the next cycle occurs again in a fresh air parcel. This cycle will be repeated during the whole 10-min period to accumulate statistically-significant data. At each period, $T_{\text{on}}$ and $T_{\text{off}}$ will be changed in a pseudo-random sequence to help get rid of trends in atmospheric parameters like the external electric field, wind, temperature, etc., when analyzing the data. The average duty cycle ($T_{\text{on}}$ / $T_{\text{off}}$) will be kept close to 50% to maximize the probability of obtaining statistically significant differences between the numbers of strikes recorded during ON and OFF times, respectively, in a binomial analysis [76].

Besides the differences in lightning strike probability during times with and without laser, several diagnostic tools will help assess the effect of the laser. The above-described interferometer based on radio-frequency antennas will provide a three–dimensional and temporally-resolved (3D+$t$) reconstruction of each individual lightning discharge, but also of more minor electric events in the thunderclouds. This reconstruction will be correlated with the laser beam path. Furthermore, each laser shot will be GPS-time-stamped with a precision better than 10 µs. These time-stamps will be correlated with the RF emission detected by the interferometer, and with the timestamped measurements of the Rogowski coils and B-dot sensors, that feature 40 µs precision. If unobstructed evidence of a discharge with sufficient intensity appears in the optical band, it should be recorded by the high-speed camera. Finally, we will evaluate whether the operation of the laser influences the probability of lightning strikes, as compared with the predictions of the above-described machine learning algorithm.

## 7 Outlook

Lightning can have a considerable economical and societal impact since it causes energy supply outages, forest

fires, damages, injury and death of humans and livestock worldwide. As climate change increases temperature gradients in the atmosphere, resulting in more frequent and severe storms [77], lightning damages are likely to increase in the future. All these factors call for the development of new approaches to lightning protection. Diverting lightning with lasers would allow the protection of industrial sites, chemical and nuclear power plants, and increase the safety of air transport, especially during the take-off and landing phases. Creating protected corridors along runways (Fig. 9) would reduce breaks in airport operation during thunderstorms, and therefore limit the associated flight delays and congestion. Furthermore, avoiding direct strikes to aircraft and airport assets would significantly reduce maintenance costs, offering a technological showcase for equipped airports. In a long term vision, laser lightning rods could be operated in conjunction with an early warning radar system locating the active regions of the thunderclouds. The laser beam would be aimed at these regions and provide optimal protection.

The authors acknowledge the European Union Horizon 2020 Research and innovation programme FET-OPEN under the grant agreement no 737033-LLR.

## Supplementary material

Video 1 : 100 ms resolution movie of a lightning strike on the Säntis tower on July 2nd, 2019, observed from the Kronberg mountain.

The Supplementary Material is available at https://www.epjap.org/10.1051/epjap/2020200243/olm.

## Author contribution statement

TP, PW, CH, AM contributed equally to this work. BE, GF, TM, KM, AM, MR, FR, JK, JPW and AH conceived the study. TP, PW, CH, AM, MM, UA, AS, MA, YBA, BM, conceived the experiments, prepared the experimental campaigns, performed the developments and experiments, and analyzed the results. All authors drafted parts of the manuscript and reviewed the full version.

## References

1. R.L. Holle, *The number of documented global lightning fatalities*, in *International Conference on Lightning Protection (ICLP 2016)* (2016), pp. 1–4
2. Lightning Costs and Losses from Attributed Sources, http://lightningsafety.com/nlsi_lls/nlsi_annual_usa_losses.htm (accessed January 8, 2020)
3. Facts + Statistics: Lightning, https://www.iii.org/fact-statistic/facts-statistics-lightning (accessed January 8, 2020)
4. Benjamin Franklin in *Pennsylvania Gazette* on October 19, 1752
5. A. Smorgonskiy, F. Rachidi, M. Rubinstein, G. Diendorfer, W. Schulz, Atmos. Res. **129–130**, 110 (2013)
6. A. Smorgonskiy, F. Rachidi, M. Rubinstein, N.V. Korovkin, A.P. Vassilopoulos, IEEE Trans. Electromagn. Compat. **59**, 1320 (2017)
7. M. Newman, J. Stahmann, J. Robb, E. Lewis, S. Martin, S. Zinn, J. Geophys. Res. **72**, 4761 (1967)
8. P. Hubert, P. Laroche, A. Eybert-Berard, L. Barret, J. Geophys. Res. Atmos. **89**, 2511 (1984)
9. D.W. Koopman, T.D. Wilkerson, J. Appl. Phys. **42**, 1883 (1971)
10. M. Miki, Y. Aihara, T. Shindo, J. Phys. D: Appl. Phys. **26**, 1244 (1993)
11. S. Uchida, Y. Shimada, H. Yasuda, S. Motokoshi, C. Yamanaka, T. Yamanaka, Z. Kawasaki, K. Tsubakimoto, J. Opt. Technol. **66**, 199 (1999)
12. S.L. Chin, S.A. Hosseini, W. Liu, Q. Luo, F. Théberge, N. Aközbek, A. Becker, V.P. Kandidov, O.G. Kosareva, H. Schroeder, Can. J. Phys. **83**, 863 (2005)
13. A. Couairon, A. Mysyrowicz, Phys. Rep. **441**, 47 (2007)
14. L. Bergé, S. Skupin, R. Nuter, J. Kasparian, J.P. Wolf, Rep. Prog. Phys. **70**, 1633 (2007)
15. J. Kasparian, J.P. Wolf, Opt. Express **16**, 466 (2008)
16. J.P. Wolf, Rep. Prog. Phys. **81**, 026001 (2017)
17. M. Rodriguez, R. Bourayou, G. Méjean, J. Kasparian, J. Yu, E. Salmon, A. Scholz, B. Stecklum, J. Eislöffel, U. Laux et al., Phys. Rev. E **69**, 036607 (2004)
18. M. Durand, A. Houard, B. Prade, A. Mysyrowicz, A. Durécu, B. Moreau, D. Fleury, O. Vasseur, H. Borchert, K. Diener et al., Opt. Express **21**, 26836 (2013)
19. X.M. Zhao, J.C. Diels, C.Y. Wang, J.M. Elizondo, IEEE J. Quantum Electron. **31**, 599 (1995)
20. D. Comtois, C. Chien, A. Desparois, F. Génin, G. Jarry, T. Johnston, J.C. Kieffer, B. La Fontaine, F. Martin, R. Mawassi et al., Appl. Phys. Lett.**76**, 819 (2000)
21. M. Rodriguez, R. Sauerbrey, H. Wille, L. Wöste, T. Fujii, Y.B. André, A. Mysyrowicz, L. Klingbeil, K. Rethmeier, W. Kalkner et al., Opt. Lett. **27**, 772 (2002)
22. B. Forestier, A. Houard, I. Revel, M. Durand, Y.B. André, B. Prade, A. Jarnac, J. Carbonnel, M.L. Nevé, J.C. de Miscault et al., AIP Adv. **2**, 012151 (2012)
23. H. Wille, M. Rodriguez, J. Kasparian, D. Mondelain, J. Yu, A. Mysyrowicz, R. Sauerbrey, J.P. Wolf, L. Wöste, Eur. Phys. J. Appl. Phys. **20**, 183 (2002)
24. J. Kasparian, M. Rodriguez, G. Méjean, J. Yu, E. Salmon, H. Wille, R. Bourayou, S. Frey, Y.B. André, A. Mysyrowicz et al., Science **301**, 61 (2003)
25. J. Kasparian, R. Ackermann, Y.B. André, G. Méchain, G. Méjean, B. Prade, P. Rohwetter, E. Salmon, K. Stelmaszczyk, J. Yu et al., Opt. Express **16**, 5757 (2008)
26. G. Méjean, R. Ackermann, J. Kasparian, E. Salmon, J. Yu, J.P. Wolf, K. Rethmeier, W. Kalkner, P. Rohwetter, K. Stelmaszczyk et al., Appl. Phys. Lett. **88**, 021101 (2006)
27. M. Shneider, A. Zheltikov, R. Miles, Phys. Plasmas **18**, 063509 (2011)
28. M. Scheller, N. Born, W. Cheng, P. Polynkin, Optica **1**, 125 (2014)
29. E. Schubert, A. Rastegari, C. Feng, D. Mongin, B. Kamer, J. Kasparian, J.P. Wolf, L. Arissian, J.C. Diels, New J. Phys. **19**, 123040 (2017)
30. F. Vidal, D. Comtois, C.Y. Chien, A. Desparois, B.L. Fontaine, T.W. Johnston, J.C. Kieffer, H.P. Mercure, H. Pepin, F.A. Rizk, IEEE Trans. Plasma Sci. **28**, 418 (2000)
31. O. Lahav, L. Levi, I. Orr, R.A. Nemirovsky, J. Nemirovsky, I. Kaminer, M. Segev, O. Cohen, Phys. Rev. A **90**, 021801 (2014)

32. Y.H. Cheng, J. Wahlstrand, N. Jhajj, H. Milchberg, Opt. Express **21**, 4740 (2013)
33. G. Point, C. Milián, A. Couairon, A. Mysyrowicz, A. Houard, J. Phys. B: At. Mol. Opt. Phys. **48**, 094009 (2015)
34. S. Tzortzakis, B. Prade, M. Franco, A. Mysyrowicz, S. Hüller, P. Mora, Phys. Rev. E **64**, 057401 (2001)
35. A. Houard, V. Jukna, G. Point, Y.B. André, S. Klingebiel, M. Schultze, K. Michel, T. Metzger, A. Mysyrowicz, Opt. Express **24**, 7437 (2016)
36. www.llr-fet.eu (2020)
37. R.W. Boyd, *Nonlinear Optics*, 3rd edn. (Academic Press, Boston, 2008)
38. P. Moulton, J. Opt. Soc. Am. B: Opt. Phys. **3**, 125 (1986)
39. C. Saraceno, D. Sutter, T. Metzger, M. Abdou-Ahmed, J. Eur. Opt. Soc.-Rapid Publ. **15**, 15 (2019)
40. K. Beil, S.T. Fredrich-Thornton, F. Tellkamp, R. Peters, C. Kränkel, K. Petermann, G. Huber, Opt. Express **18**, 20712 (2010)
41. A. Giesen, H. Hügel, A. Voss, K. Wittig, U. Brauch, H. Opower, Appl. Phys. B **58**, 365 (1994)
42. T. Gottwald, V. Kuhn, S.S. Schad, C. Stolzenburg, A. Killi, *Recent developments in high power thin disk lasers at TRUMPF Laser*, in *Technologies for Optical Countermeasures X; and High-Power Lasers 2013: Technology and Systems* (International Society for Optics and Photonics, 2013), Vol. 8898, p. 88980P
43. S.S. Schad, In preparation, Private communication from April 9th, 2020
44. T. Dietz, D. Bauer, M. Scharun, H. Hock, D. Sutter, A. Killi, A. Leitenstorfer, *Monolithic multi-pass thin-disk laser amplifier providing near fundamental mode 2.3 mJ pulse energy at 1.4 kW average output power and 950 fs pulse duration*, in *Advanced Solid State Lasers* (Optical Society of America, 2018), pp. AM2A–4
45. T. Dietz, M. Jenne, D. Bauer, M. Scharun, D. Sutter, A. Killi, Opt. Express **28**, 11415 (2020)
46. T. Metzger, C.Y. Teisset, F. Krausz, *High-repetition-rate picosecond pump laser based on an Yb: YAG disk amplifier for optical parametric amplification*, in *Advanced Solid-State Photonics* (Optical Society of America, 2008), p. TuA2
47. P. Krötz, C. Wandt, C. Grebing, C. Herkommer, R. Jung, S. Klingebiel, S. Prinz, C.Y. Teisset, K. Michel, T. Metzger, *Towards 2 kW, 20 kHz ultrafast thin-disk based regenerative amplifiers*, in *Advanced Solid State Lasers* (Optical Society of America, 2019), pp. ATh1A–8
48. S. Klingebiel, M. Schultze, C.Y. Teisset, R. Bessing, M. Häfner, S. Prinz, M. Gorjan, D. Sutter, K. Michel, H.G. Barros et al., *220 mJ Ultrafast Thin-Disk Regenerative Amplifier*, in *CLEO: Science and Innovations* (Optical Society of America, 2015), pp. STu4O–2
49. E. Treacy, IEEE J. Quantum Electron. **5**, 454 (1969)
50. C. Herkommer, P. Krötz, S. Klingebiel, C. Wandt, D. Bauer, K. Michel, R. Kienberger, T. Metzger, *Towards a Joule-Class Ultrafast Thin-Disk Based Amplifier at Kilohertz Repetition Rate*, in *2019 Conference on Lasers and Electro-Optics (CLEO)* (IEEE, 2019), pp. 1–2
51. C. Herkommer, P. Krötz, R. Jung, S. Klingebiel, C. Wandt, R. Bessing, P. Walch, T. Produit, K. Michel, D. Bauer et al., Opt. Express **28**, 30164 (2020)
52. D.F. Hotz, Appl. Opt. **4**, 527 (1965)
53. K. Murari, H. Cankaya, P. Kroetz, G. Cirmi, P. Li, A. Ruehl, I. Hartl, F.X. Kärtner, Opt. Lett. **41**, 1114 (2016)
54. S. Klingebiel, C. Wandt, M. Siebold, Z. Major, I. Ahmad, S. Trushin, R. Hörlein, T.J. Wang, F. Krausz, S. Karsch, *Counteracting gain narrowing using spectral amplitude shaping in a high-energy diode-pumped CPA system based on Yb-doped materials*, in *Advanced Solid-State Photonics* (Optical Society of America, 2009), p. TuB9
55. T. Produit, P. Walch, G. Schimmel, B. Mahieu, C. Herkommer, R. Jung, T. Metzger, K. Michel, Y.B. André, A. Mysyrowicz et al., Opt. Express **27**, 11339 (2019)
56. Y.P. Raizer, Sov. Phys. Uspekhi **8**, 650 (1966)
57. O. Chalus, A. Sukhinin, A. Aceves, J.C. Diels, Opt. Commun. **281**, 3356 (2009)
58. P.Q. Elias, N. Severac, J.M. Luyssen, Y.B. André, I. Doudet, B. Wattellier, J.P. Tobeli, S. Albert, B. Mahieu, R. Bur et al., Sci. Adv. **4**, eaau5239 (2018)
59. K. Berger, Electra **41**, 23 (1975)
60. C. Romero, F. Rachidi, M. Paolone, M. Rubinstein, IEEE Trans. Power Deliv. **28**, 1804 (2013)
61. Wikimedia Commons, the free media repository - File: SäntisLuftbild.JPG https://commons.wikimedia.org/w/index.php?title=File:SäntisLuftbild.JPG&oldid=278731957 (accessed May 26, 2020)
62. C. Baum, Sensor and Simulat. Not. **8**, 218 (1964)
63. C. Baum, E. Breen, J. Giles, J. O'Neill, G. Sower, IEEE Trans. Antennas Propag. **26**, 22 (1978)
64. M. Azadifar, M. Paolone, D. Pavanello, F. Rachidi, V. Rakov, C. Romero, M. Rubinstein, *An update on the charaterictics of positive flashes recorded on the Säntis Tower*, in *2014 International Conference on Lightning Protection (ICLP)* (IEEE, 2014), pp. 777–781
65. M. Stock, M. Akita, P. Krehbiel, W. Rison, H. Edens, Z. Kawasaki, M. Stanley, J. Geophys. Res. Atmos. **119**, 3134 (2014)
66. M. Azadifar, F. Rachidi, M. Rubinstein, M. Paolone, G. Diendorfer, H. Pichler, W. Schulz, D. Pavanello, C. Romero, J. Geophys. Res. Atmos. **121**, 595 (2016)
67. L. He, M. Azadifar, F. Rachidi, M. Rubinstein, V.A. Rakov, V. Cooray, D. Pavanello, H. Xing, J. Geophys. Res. Atmos. **123**, 4045 (2018)
68. C. Romero, F. Rachidi, M. Rubinstein, M. Paolone, V.A. Rakov, D. Pavanello, J. Geophys. Res. Atmos. **118**, 12 (2013)
69. D. Li, M. Azadifar, F. Rachidi, M. Rubinstein, M. Paolone, D. Pavanello, S. Metz, Q. Zhang, Z. Wang, IEEE Trans. Electromagn. Compat. **58**, 161 (2015)
70. M. Azadifar, D. Li, F. Rachidi, M. Rubinstein, G. Diendorfer, W. Schulz, H. Pichler, V.A. Rakov, M. Paolone, D. Pavanello, J. Atmos. Sol. - Terr. Phys. **159**, 48 (2017)
71. M. Azadifar, F. Rachidi, M. Rubinstein, V.A. Rakov, M. Paolone, D. Pavanello, S. Metz, J.Geophys. Res. Atmos. **121**, 6425 (2016)
72. A. Mostajabi, D.L. Finney, M. Rubinstein, F. Rachidi, npj Clim. Atmos. Sci. **2**, 1 (2019)
73. E.L. Dawes, J.H. Marburger, Phys. Rev. **179**, 862 (1969)
74. I.S. Golubtsov, V.P. Kandidov, O.G. Kosareva, Quan. Electron. **33**, 525 (2003)
75. Art. 10b of the Ordonnance relative à la loi fédérale sur la protection contre les dangers liés au rayonnement non ionisant et au son, https://www.admin.ch/opc/fr/classified-compilation/20173129/index.html (accessed October 21, 2019)
76. R. Ackermann, K. Stelmaszczyk, P. Rohwetter, G. Méjean, E. Salmon, J. Yu, J. Kasparian, G. Méchain, V. Bergmann, S. Schaper et al., Appl. Phys. Lett. **85**, 5781 (2004)

77. IPCC, *Climate change 2014: Impacts, Adaptation and Vulnerability. Contribution of the Working Group II to the Fifth Assessment Report of the Intergovernmental Panel on Climate Change* (Cambridge University Press, Cambridge, UK, and New-York, NY, USA, 2014)



**Cite this article as:** Thomos Produit, Plerre Walch, Clemens Herkommer, Amlrhosseln Mostajabi, Michel Moret, Ugo Andral, Antonlo Sunjerga, Mohammad Azadifar, Yves-Bernard André, Benoît Mahieu, Walter Haas, Bruno Esmiller, Gilles Fournier, Peter Krötz, Thomos Metzger, Knut Michel, André Mysyrowicz, Marcos Rubinstein, Farhad Rachidi, Jérôme Kasparian, Jean-Pierre Wolf, Aurelien Houard, The laser lightning rod project, Eur. Phys. J. Appl. Phys. **93**, 10504 (2021)